



Seasonal to decadal variability in ice discharge from the Greenland Ice Sheet

Michalea D. King^{1,2}, Ian M. Howat^{1,2}, Seongsu Jeong³, Myoung J. Noh¹, Bert Wouters^{4,5}, Brice Noël⁴, and Michiel R. van den Broeke⁴

5 ¹Byrd Polar and Climate Research Center, Columbus, USA.

²School of Earth Sciences, Ohio State University, Columbus, USA.

³Department of Earth System Science, University of California, Irvine

⁴Institute for Marine and Atmospheric research Utrecht, Utrecht University, Utrecht, Netherlands.

⁵Civil Engineering and Geosciences, Delft University of Technology, Delft, Netherlands

10

Correspondence to: Michalea D. King (michaleaking@gmail.com)

Abstract. Rapid changes in thickness and velocity have been observed at many marine-terminating glaciers in Greenland, impacting the volume of ice they export, or discharge, from the ice sheet. While annual estimates of ice-sheet wide discharge have been previously derived, higher-resolution records are required to fully constrain the temporal response of these
15 glaciers to various climatic and mechanical drivers that vary in sub-annual scales. Here we derive the first continuous, ice-sheet wide record of total ice sheet discharge for the 21st century resolving a seasonal variability of 6 %. The amplitude of seasonality varies spatially across the ice sheet from 5 % in the southeastern region to 9 % in the northwest region. We analyze seasonal to annual variability in the discharge time series with respect to both modelled meltwater runoff, obtained from RACMO2.3p2, and glacier front position changes over the same period. We find that year-to-year changes in total ice
20 sheet discharge are related to annual front changes ($r^2 = 0.59$, $p = 10^{-4}$) and that the annual magnitude of discharge is closely related to cumulative front position changes ($r^2 = 0.79$), which show a net retreat of > 400 km, or an average retreat of > 2 km at each surveyed glacier. Neither maximum seasonal runoff or annual runoff totals are correlated to annual discharge, which suggests that larger annual quantities of runoff do not relate to increased annual discharge. Discharge and runoff, however, follow similar patterns of seasonal variability, with near-coincident periods of acceleration and seasonal maxima.
25 These results suggest that changes in glacier front position drive secular trends in discharge, whereas the impact of runoff is likely limited to the summer months when observed seasonal variations are substantially controlled by the timing of meltwater input.



1 Introduction

Mass loss from the Greenland Ice Sheet (GrIS) is now the single largest cause of sea level rise (Vaughan et al. 2013),
30 contributing approximately 1 mm a^{-1} of global water equivalent over the 2010–2015 period (van den Broeke et al. 2016). Since the mid 1990's, the GrIS has been losing ice at an increasing rate (Rignot et al. 2011; Sasgen et al. 2012; Hanna et al.



2013; Enderlin et al. 2014) due in part to increased discharge from marine-terminating outlet glaciers (Rignot and Kanagaratnam, 2006; Rignot et al. 2008; Enderlin et al. 2014). Substantial increases in ice discharge are observed at large outlet glaciers over periods of months or less (e.g. Joughin et al., 2004; Howat et al. 2005), demonstrating short term sensitivity to external drivers, such as ocean circulation (Straneo et al. 2013; Walsh et al. 2012) melt runoff (Joughin et al. 2008; Andersen et al. 2011), and sea ice/mélange conditions near the calving front (Howat et al. 2010; Moon et al. 2015; Bendtsen et al. 2017). Thus, understanding the dynamics of these glaciers requires measurements with a high temporal resolution.

Seasonal variability in the flow speed of marine-terminating glaciers in Greenland has been observed for small samples of glaciers (Howat et al. 2010; Howat et al. 2011) and for larger glacier inventories over short time periods (Moon et al. 2014; Moon et al. 2015). Previous ice sheet-wide estimates of discharge were largely based on summertime velocities and, therefore, may be biased toward higher values, demonstrating the need for a longer record of ice sheet-wide discharge that resolves short term variability, potentially associated with surface meltwater runoff and calving. Here we present the first continuous record of net ice sheet discharge, derived over the 2000–2016 period. This record is used to resolve both distinct ice-sheet wide and regional patterns of seasonal variability and evaluate how seasonality has changed through time. We then compare these records to modelled meltwater runoff data and records of glacier front positions to assess how these terms impact discharge on seasonal to annual time scales.

2 Data and Methods

Following Howat et al. (2011), we derive time series of the rate of solid ice discharge (D) for each glacier by integrating the product of glacier thickness, ice velocity, and ice density across the glacier width at the grounded terminus. Observations are sampled along a static profile, i.e. fluxgate, oriented perpendicular to the direction of flow and located upstream of the grounding line, immediately inland of the most retreated grounding line during the 2000–2016 study period. We use the same flux gates as Howat et al. (2011) and Enderlin et al. (2014) except in cases where the grounding line had retreated inland of the gate location. Further, while Enderlin et al. (2014) used empirical relationships to estimate cross-sectional area and discharge at glaciers for which only along-flow profiles or no bed topography were available, we use the BedMachine version 3 gridded bed topography dataset (Ligheem et al. 2017), which uses ice thickness, flow speed observations and surface mass balance (SMB), which is the sum of the mass gained from accumulation and lost due to meltwater runoff, sublimation and snow drift erosion, to constrain a mass conservation model. As in prior studies, we assume that changes in the elevation of the glacier bed, due to erosion, deposition and/or lithosphere displacement, are small, as are variations in ice flow velocity with depth in fast flowing ($> 1 \text{ km a}^{-1}$) glaciers. Thus, discharge is estimated from the bed topography and repeat measurements of surface elevation, the difference of which provides the time-variable ice thickness, and ice flow



velocity. Additional information regarding the placement of flux gates and descriptions of the datasets are provided in the supplementary material.


Enderlin et al. (2014) derived annual discharge estimates from, mo velocity data collected between April and September.
5 Increased data collection by SAR sensors (Terra/TandemSAR-X), low-light level functionality of Landsat 8 (Jeong and Howat, 2015; Fahnestock et al. 2016), and increased sampling density using image pairs between multiple sensors and/or acquired from crossing orbital tracks (Rosenau et al. 2015; Jeong et al. 2017), enable substantially better temporal resolution than available for Enderlin et al. (2014). Thus, we combine this increased velocity sampling with a Kalman filter approach to estimate D and its uncertainty as a continuous series. For each glacier, we first derive a standard seasonality curve by
10 detrending the time series of monthly mean speeds and grouping mean speeds by the month of year, so that a 17-year time series would provide up to 17 estimates of mean speed for a given month. The standard seasonality is then obtained from the median value and covariance of the observations for each month. Months with fewer available observations will therefore tend to have a higher range of uncertainty. If no optical or radar data exist for a particular month throughout the time series, a standard monthly value is estimated by fitting a periodic function to the available monthly median values. The seasonality
15 curve is then normalized to yield an estimate of fractional change in speed between months, which informs a simple linear model. Within the Kalman filter framework, this linear model assimilates the observations to optimize estimates for missing months of the time series, with the errors equal to the combination of the observation and prediction errors. Uncertainty in the seasonality curves tend to exceed observational errors, resulting in formal errors that increase with distance from the observations. A more detailed description of this approach is provided in the supplementary material. Velocity
20 measurements for the four northernmost glaciers (Steenby, C.H. Ostefeld, Academy, and Hagen Brae) were too sparse to derive a continuous time series and we instead estimate an annual D for these glaciers.

We use the same repeat ice surface elevation dataset as Enderlin et al. (2014), extended through 2016, and with the addition of stereoscopic digital elevation models produced from sub-meter resolution DigitalGlobe Inc. WorldView imagery for the
25 ArcticDEM project (www.arcticdem.org). The DEMs are produced to 2 m resolution and coregistered over stationary (exposed rock) surfaces using the algorithm of Noh and Howat (2014). Following coregistration to remove biases, these data have an accuracy of better than ± 0.5 m (Noh and Howat, 2015). Elevation profiles are filtered for noise and smoothed as described in the supplementary material before subtracting the BedMachine V3 bed profiles from each surface elevation profile to give ice thicknesses. The series of ice thickness estimates were then linearly interpolated to the times of the series
30 of velocity observations to obtain ice discharge rate, D . Errors in discharge at velocity observation times are calculated from propagation of measurement errors and uncertainties of interpolated values are determined from a Monte Carlo ensemble, as described in the supplementary material. We derive total ice sheet mass balance over the 2000–2016 period by combining our estimates of D with SMB data obtained from a 5.5 km simulation of the Regional Atmospheric Climate Model, RACMO2.3



version 2 (RACMO2.3p2) statistically downscaled to 1 km, and compare these totals to monthly satellite gravimetry observations of ice sheet mass balance from the Gravity Recovery and Climate Experiment (GRACE).

While RACMO2.3p2 applies the same model physics as described in Noël et al. (2018), a twice finer horizontal resolution (5.5 km instead of 11 km) better resolves SMB gradients over narrow glaciers at the ice sheet margins. Based on comparison
5 with observations, the uncertainty in modelled basin-integrated runoff and snow accumulation (total precipitation minus sublimation) are, respectively, 20 % and 10%, which are combined to obtain an uncertainty in SMB by assuming the two are independent of each other (Noël et al., 2018; Van As et al., 2018).

We examine how D varies in response to meltwater runoff and changes glacier front position. Daily meltwater runoff
10 estimates are also obtained from the RACMO2.3p2 product. Daily runoff values at each model grid point are summed over the ice sheet and within regional basins for comparison to D . We measure relative changes in glacier front position manually for the period 2000–2016 using all available imagery from ASTER and LANDSAT 4–8. This resulted in a measurement frequency of up to every few days during the summer, declining in frequency during the polar night, especially prior to 2012 (Landsat 8 launch). Due to the very large quantity of measurements, we used the efficient centerline methodology described
15 in Walsh et al. (2012), who found a negligible difference in the temporal variation of front position between this and methods that involve digitization of the entire front. To enable comparison with discharge and runoff time series, we convert the irregular front position observations to daily rates of change and then resample the rates at 7-day intervals. The new resampled subset is then linearly interpolated to daily rates of front position change over the study period. Individual glacier records of frontal change are combined into regional and GrIS-wide records by first applying a discharge-dependent
20 weighting function, so that retreat and advance events at larger glaciers are weighted more heavily, due to the proportionally larger impact of these glaciers on the discharge time series. We do not include front position measurements for Zachariae Isstrøm and 79Fjorden because the perennial mélange of tabular icebergs at their fronts make delineation of the front position arbitrary (e.g. Moon et al. 2008). 

3 Results

25 3.1 Net Ice Sheet Discharge and Mass Balance

The net GrIS-wide D reveals a clear seasonality, typically characterized by an annual minimum in December and a maximum in mid-July (Figure 1), superimposed upon multi-year variability. Removing the linearly-interpolated annual means from the time series gives an average seasonal amplitude of 30 Gta^{-1} , or approximately 6 % of the mean annual discharge. The seasonal amplitude was largest in 2002, 2004, and 2005, reaching up to 46 Gta^{-1} , and, on average, higher
30 before 2005 ($35 \pm 8 \text{ Gta}^{-1}$, where the uncertainty is $1-\sigma$). This compares to an average seasonal amplitude of $27 \pm 4 \text{ Gta}^{-1}$ after 2006, with overall trend of -0.7 Gta^{-1} from 2000 to 2016. Beginning from a mean annual discharge of $440 \pm 8 \text{ Gta}^{-1}$ in



2000, D increases to a maximum of $524 \pm 9 \text{ Gta}^{-1}$ in late June 2005, primarily due to the accelerations of Kangerdlugssuaq and Helheim glaciers in the east (Howat et al. 2007; Joughin et al. 2008). In the following two years, the rapid decrease in D from these two glaciers resulted in the greatest seasonal decrease in GrIS D in 2006, declining to a minimum of $461 \pm 9 \text{ Gta}^{-1}$ by January 2008. D then gradually increased, reaching the second-highest time series annual maximum of $494 \pm 6 \text{ Gta}^{-1}$ in 2015, with a peak summertime value of $511 \pm 6 \text{ Gta}^{-1}$ in July 2015. Annual D declined by 5 Gta^{-1} in 2016 largely due to reductions in discharge observed at Køge Bugt and Jakobshavn (Figure S3). Thus, D has remained consistently between 10 to 12 % above the 2000 rates since 2010. Along with the annual mean quantities, the seasonal discharge signal varies throughout the study period. Prior to 2013, the seasonal variation in D is relatively symmetric, with a single distinct peak and little variability on sub-annual timescales. The final four years of the record are more variable, with minor peaks following the seasonal maxima. This pattern is predominantly due to changes observed in the NW region, addressed in detail in Sect. 3.2.

The ice sheet's four largest glaciers (Fig. S3) together account for 25 % of the total D , and 56 % of the cumulative anomaly in GrIS-wide D relative to annual D in 2000. Variations in these four glaciers, therefore, dominate variability in total GrIS D . The secular trend of the combined D is substantially different with the four largest glaciers removed (Figure S4). Following the decline in D between 2005 and 2008, the combined D of the remaining glaciers, denoted here as D_s , continued to increase, reaching a maximum in 2011 before declining to another minimum 2012. The seasonal decline in D_s during the winter of 2013–2014 was anomalously shallow, with speeds remaining elevated across the ice sheet. D_s then increased to a record maximum in July 2015, reaching an annual maximum of $374 \pm 5 \text{ Gta}^{-1}$ in 2016. Thus, an overall continued increase in D_s since 2008 was largely offset in declines from the four largest glaciers over that period. Removing the four largest glaciers, however, does not change the relative seasonal amplitude of approximately 6 %, indicating that GrIS-wide seasonality is not dependent on the largest glaciers.

Our continuous estimates of D enable the first direct comparison to monthly satellite gravimetry observations of ice sheet mass balance from GRACE. We compute ice sheet mass balance by subtracting our estimates of net GrIS-wide D from daily 1 km^2 resolution SMB estimates obtained from RACMO2.3p2 (Noël et al., 2018). Following the methodology of van den Broeke et al. (2016), we incorporate SMB fluxes from the ice-free tundra and peripheral ice caps, which are included in the GRACE signal, into the ice-sheet mass balance calculations. Mass balance estimates of peripheral ice caps derived from laser altimetry (Bolch et al. 2013) found that areal averaged mass losses were similar for land-terminating and marine-terminating glaciers, and thus we assume D from peripheral glaciers and ice caps is small relative to the errors in other terms. We remove the SMB over ice shelves, downstream of the discharge flux gates, from the total. We use GRACE ice sheet mass updated from Wouters et al. (2013), corrected for glacial isostatic adjustment using the model of Khan et al. 2016. The cumulative mass losses estimated by $\text{SMB} - D$ and GRACE, calculated by taking the difference between the annual mean cumulative losses in 2016 and 2003, are 3263 ± 259 and $3479 \pm 280 \text{ Gt}$, respectively, over the 2003–2016 period (Figure 2).



This 7% difference equates to an integrated monthly bias of less than 1.5 Gt, nearly all of which is due to a greater loss estimated by GRACE in the anomalously severe 2011 and 2012 melt seasons. Extended to the beginning of the D time series, we estimate a total cumulative mass loss from 2000 through 2016 of 3730 ± 277 Gt. We also delineate individual glacier D records and SMB totals to align with the six regional basins used in Wouters et al. (2013) and compare these quantities to basin-scale GRACE estimates (Table 1, and Figures S5, S6). We find that while the seasonal variability in mass loss shown in GRACE is well resolved by SMB – D estimates for all basins, the level of agreement in magnitude of cumulative mass loss varies by basin. Estimates agree within their combined uncertainty ($< \pm 10$ Gt $^{-1}$) for three basins, which together account for $\sim 65\%$ of the total mass loss. Annual mass loss rates from SMB – D in Basin 1 and 2 (northern regions) exceed GRACE estimates rates by more than 50 %, and mass loss rates from GRACE are approximately double those from SMB – D in Basin 4 (southeast). These differences largely cancel each other out, leading to the close agreement between estimates for the GrIS as a whole.

3.2 Regional Discharge Variability

Partitioning D into the four quadrants used by Enderlin et al. (2013), we find significant spatial variability (Figure 3a), with regional D quantities summarized in Table 2. The northwestern (NW) region, which includes Jakobshavn northward to and including Petermann Glacier, has the highest combined discharge, averaging 207 Gt $^{-1}$, with a cumulative discharge anomaly, defined as the cumulative difference from the year 2000 D , of 343 ± 21 Gt. In the NW, we also find the highest seasonal amplitude in D of 18 ± 3 Gt $^{-1}$ or 9 %, with Jakobshavn Glacier (Figure S3A) alone contributing 7 ± 3 Gt $^{-1}$. Removing this glacier from the sample reduces the fractional seasonal amplitude to the GrIS-wide average of 6 % (10 ± 1.7 Gt $^{-1}$). On average, maximum D occurs on 12 July (day 192) with a uniform, sinusoidal seasonal cycle transitioning to an irregular, saw tooth pattern in 2012. This shift is also visible in the GrIS-wide time series and is primarily due to the emergence of a secondary, mid to late autumn peak in D at Jakobshavn (Figure S3A). On average, D at Jakobshavn reaches a seasonal maximum ~ 1 week later than the NW regionally averaged maxima. We find no significant trend in the timing of the seasonal maximum in the NW.

The southeastern (SE) region, extending northward to and including Kangerdlugssuaq glacier, had a cumulative D anomaly of 284 ± 17 Gt since 2000 (Figure 3b). Approximately 60 % of the cumulative anomaly occurred at Helheim and Kangerdlugssuaq, due to the rapid 2004–2005 terminus retreat and subsequent acceleration (Howat et al. 2007), resulting in the SE reaching a period maximum rate of D of 238 ± 4 Gt $^{-1}$ in June 2005. Following this period of acceleration, regional D values steadily declined to an annual average of 187 ± 4 Gt $^{-1}$ in 2016, within the error of D observed in 2000 (182 ± 6 Gt $^{-1}$), prior to acceleration. As discovered by Enderlin et al. (2014), an overall decreasing trend in SE D of -1.7 Gt $^{-2}$ after 2005 has partially offset the overall increase of 2.7 Gt $^{-2}$ in the NW. Despite a large net regional D , there is substantially less



seasonal variation in the SE, with an average seasonal amplitude of $9 \pm 5 \text{ Gta}^{-1}$ or 5 %. The seasonal amplitude was greater during the 2000–2005 period of acceleration ($14 \pm 6 \text{ Gta}^{-1}$) than during the 2006–2016 period ($7 \pm 2 \text{ Gta}^{-1}$). The three largest glaciers in this region (Køge Bugt, Helheim, and Kangerdlugssuaq) together contribute approximately 40 % of the net regional D . A seasonal signal is more visible after 2005 when excluding these three glaciers, with the remaining glaciers showing a slightly larger seasonal amplitude of approximately 6 %. On average, the summertime seasonal maxima in D occur approximately one week earlier in the SE than in the NW.

The NE and SW regions have fewer marine terminating outlet glaciers and contribute less to the total GrIS D . Discharge from the northeast (NE) region (Figure 3c), contributes approximately 12 % of the total ice sheet D , with the regional ice flux dominated by Zachariæ Isstrøm and 79Fjorden Glacier. This region exhibits a relatively consistent seasonal variability of $5 \pm 1 \text{ Gta}^{-1}$, or 8 %. The seasonal maximum typically occurs at the end of June. Annual D increased by 4 Gta^{-1} between 2013 and 2016, largely due to increased D observed at Zachariæ Isstrøm (Mouginot et al. 2015; Choi et al. 2017). D in the NE shows a steady increase, accelerating from a rate of $\sim 0.2 \text{ Gta}^{-2}$ during 2000–2012 to over 1 Gta^{-2} during the 2013–2016 period, entirely due to acceleration of Zachariæ Isstrøm and 79Fjorden glaciers. Lastly, only 7 glaciers constitute the southwest (SW) (Figure 3d), where land-terminating glaciers dominate the margin. Kangia glacier alone accounts for over approximately 60 % of the total SW regional D . A doubling of the seasonal amplitude at Narssap Glacier, coinciding with rapid terminus retreat (Motyka et al. 2017), is responsible for the increase in regional variability after 2011.

As mentioned above, variations in D may be due primarily to the largest glaciers, which may or may not represent typical glacier behavior. To assess seasonal glacier dynamics, we remove the impact of glacier size by first subtracting the secular trend from the series and then normalizing each glacier's detrended D series by its maximum seasonal amplitude. This process effectively creates equally-weighted time series of D for individual glaciers, while isolating the seasonal signal. The averages of the normalized seasonal discharge for each region and the total GrIS are shown in Figure 4 and reveal that a distinct seasonal signal is a ubiquitous feature across the ice sheet, independent of glacier size. However, the timing of the seasonal maxima in the normalized data occurs approximately ten days earlier (late June, typically) than without normalization. As before, there is also a decrease in seasonal amplitude since 2013 of 20 % relative to earlier years. We observe a similar decrease in amplitude in the normalized series for the SE, NW and NE. This widespread reduction in seasonal amplitude corresponds with a period of relatively stable mean annual D , as shown in Fig. 1. As was noted from the raw regional D , the SE region exhibits the smallest seasonal variability. Unlike the raw time series, which showed the greatest seasonal amplitude in the NW, the NE region shows the largest seasonal amplitude in the normalized time series. This is likely due to the reduced impact of Jakobshavn on NW seasonality through the normalization. Fig. 4 also shows that the seasonal maxima occur coincidentally for the majority of glaciers over the majority of the GrIS, with the few glaciers in the SW reaching a seasonal maximum slightly earlier than the GrIS-wide average.



3.3 Variations in Annual Discharge, Front Position and Runoff

We expect that D will vary with both ice front position, due to changes in resistive stress at the terminus (e.g. Thomas et al. 2004; Howat et al. 2008), and with seasonal meltwater runoff, due to variations in basal water pressure (e.g. Jourdain et al., 2012). We first test for broad, linear correlations between annual discharge, both over the entire GrIS and regionally, and annual changes in front position and total runoff. We calculate the GrIS-wide and regional annual runoff totals from daily RACMO2.3p2 outputs. Ice sheet-wide and regional front positions are the sum of each glacier's change between 1 January each year, weighted by the fractional contribution of the glacier's D to the GrIS or regional total. We then divide these sums by the total number of glaciers across the GrIS or region of interest and express the quantity as the mean weighted position change.

5

For the entire GrIS, we find the strongest relationship between annual D and the weighted, cumulative change in 1 January front position ($r^2 = 0.79$, $p = 10^{-6}$) (Figure 5A). This correlation is slightly stronger than that obtained between annual D and the cumulative front position change from the previous year ($r^2 = 0.68$, $p = 10^{-4}$). A weaker, but significant correlation is found between the change in annual D , defined here as the difference between the current and previous year's annual D , and annual front position change during both the current year ($r^2 = 0.59$, $p = 0.0005$) (Figure 5B) and the previous year ($r^2 = 0.50$, $p = 0.002$). These correlations are strengthened by excluding Petermann Glacier, where large retreats of its uniquely thin and fractured ice shelf in 2010 and 2012 had no resolvable impact on ice flow speed and, thus, D (Lemos et al. 2018; Münchow et al., 2014). In contrast, no significant correlation is found between annual D and total annual runoff. The addition of annual runoff as an independent variable also does not improve the correlations with front position described above.

10

Retreat was widespread in the study period in the NW, with glaciers there retreating, on average, 2.8 km from 2000 to 2017. The cumulative, weighted regional front position change shows a near-linear annual retreat with small interannual variation. A similarly strong linear trend is present in annual D , resulting in a nearly perfect correlation with annual cumulative front position change ($r^2 = 0.92$, $p = 10^{-9}$). This relationship is slightly strengthened at a one-year lag, with a correlation of $r^2 = 0.94$ ($p = 10^{-9}$) between annual D and cumulative front position up through the previous year. Only a weakly significant ($r^2 = 0.25$, $p = 0.048$) relationship exists between the change in NW annual D and the annual, rather than cumulative, front change during the previous year. Retreat also dominated in the SE region over the study period, averaging 1.7 km. Unlike in the NW, however, D in the SE correlated to the annual weighted change in front position, rather than cumulative change. Annual D is significantly correlated to the previous year's annual front position change ($r^2 = 0.28$, $p = 0.033$). Even stronger is the correlation between the change in annual D and the annual front position change of the previous year, ($r^2 = 0.60$, $p = 10^{-4}$) (Figure S7). As with the complete GrIS, no significant correlations are found between D or interannual change in D and annual runoff in either the SE or NW regions.

20

25

30



3.4 Seasonal Variations in Discharge, Front Position and Runoff

Runoff on the ice sheet typically begins in May and continues through September, reaching a maximum daily rate in July. Smoothing daily runoff values with a monthly (31-day) running mean results in a seasonal distribution with one or several distinct peak(s). Comparing GrIS-wide D to the smoothed runoff series (Figure 6), we find that seasonal acceleration of D is greatest at the onset of runoff, and reaches a seasonal maximum, on average, 13 ± 9 days after the greatest increase in runoff and 12 ± 7 days before the seasonal maximum in runoff. The only exception to this progression was in 2013, when the peak in D occurred after the seasonal maximum in runoff. The maximum D occurs, on average, 40 ± 8 days after the onset of significant runoff. Since the distribution of daily runoff includes a long tail of small values, we define the significant runoff onset as the day when runoff exceeds the 50th percentile of daily runoff values between April 1 and November 1. Using this threshold, we find a significant correlation between the date of runoff onset and the date of maximum D ($r^2 = 0.33$, $p = 0.015$), indicating that a later onset in runoff tends to correlate with a later peak in D . However, despite the near synchronous timing between seasonal peaks in runoff and D , we find no other significant relationships between the timing of runoff and discharge, nor between the magnitude of runoff and the magnitude of the seasonal maximum D , or total annual D .

There is regional variability in the timing and amplitude of runoff. The NW region reaches an average maximum of 2.6 ± 0.5 Gt day⁻¹ on day 199 (± 8), totaling 82 ± 21 Gt annually. Significant runoff onset occurs in early June (day 160 ± 7), one week later than runoff in the SE (day 15 ± 8) and preceding the timing of the regional maximum D by approximately one month (32 ± 10 days). There is a significant relationship in the NW region between the timing of runoff onset and the timing of the seasonal maximum in D ($r^2 = 0.46$, $p = 0.003$). In the SE, there is a similar magnitude of total annual runoff (75 ± 16 Gt), but a substantially lower maximum daily rate of 1.7 ± 0.5 Gt day⁻¹ which occurs, on average, on day 208 (± 10). There is also a greater interannual variability in the temporal separation between onset of runoff and maximum D (33 ± 22 days) in the SE region and, as a result, there is no significant correlation in their timing. As with the GrIS as a whole, we find no significant relationships between the magnitudes of runoff and D , or total annual D , in either region.

Front position also varies seasonally. Integrated over the GrIS, net weighted retreat begins in early April (day 92 ± 33) and continues through the end of September (day 265 ± 17). Daily rates of retreat increase most rapidly in early June (day 153 ± 41), reaching, on average, a maximum retreat rate on day 180 (± 35). We test for linear relationships between the timing of initial retreat and greatest increase in retreat, and timing and magnitude of maximum daily rate of retreat with the same seasonal D metrics described above (e.g. magnitude and timing of maximum D and timing of greatest increase in D). We find no significant relationships between the timing or magnitude of seasonal frontal change quantities with seasonal D . The seasonal progression of retreat and advance occurs earlier in the NW relative to the GrIS-wide average. In this region, total weighted front change rates show the greatest increase in retreat in mid-May, on average, (day 135 ± 46), and reach a peak retreat rate in mid-June (day 167 ± 38). In the SE region, by contrast, retreat accelerates the most in mid-June (day 169 ± 46)



and reaches a maximum rate on day 200 (± 23). As with the GrIS-wide results, we find no significant correlations between the seasonality of retreat and D at the regional scale.

4 Discussion

5 Our GrIS-wide estimate of D in 2000 ($440 \pm 8 \text{ Gta}^{-1}$) is approximately 5 % and 20 % lower than annual estimates derived for
2000 in Enderlin et al. (2014) and Rignot et al. (2011), respectively. Our 2003–2010 mean D of $484 \pm 9 \text{ Gta}^{-1}$ agrees within
margins of uncertainty to estimates by Kjeldsen et al. (2015) over the same time period ($465 \pm 65.5 \text{ Gta}^{-1}$), with a bias of less
than 20 Gta^{-1} . Approximately half of the difference from Enderlin et al. (2014) can be explained by the bias resulting from
the use of, mostly, summertime medians in that study. Other differences likely are due to a combination of observational
10 error, uncertainties associated with empirical assumptions made in the absence of ice thickness data, methodological
differences in the processing and filtering of surface elevation data, and uncertainties associated with ice thickness
derivations using hydrostatic equilibrium assumptions (Rignot et al. 2011). The higher temporal resolution of D presented
here also avoids nonuniform temporal sampling biases, and, once combined with SMB data from RACMO2.3p2, is in close
agreement with independent estimates of ice sheet mass balance from GRACE. Significant discrepancies, however, between
15 the SMB – D and GRACE estimates still exist at the regional scale, with SMB – D predicting nearly twice the loss in north
of the ice sheet, but approximately half the loss of GRACE in the south. The difference in the SE may be due to an
underestimation of either runoff, partly from the high slope of the ablation zone, overestimated accumulation rates, or ice
thickness for glaciers lacking radio echo sounding measurements near the terminus. The differences in the north may be due
to unrealistically low net SMB predicted there by RACMO2.3p2, with some years showing zero or negative SMB, and
20 cumulative SMB loss in region 1 (Figure S6).

The seasonal variation in D of 6 % is significantly less than the ~ 10 % typically assumed for the GrIS (e.g. Rignot and
Kanagaratnam, 2006; Andersen et al. 2015). While individual regions have larger relative seasonal variations, differences in
the timing of their peaks cause them to offset each other in total. For instance, the GrIS-wide seasonal amplitude would be
25 60 Gta^{-1} , or nearly 13 %, if the seasonal signals expressed at individual glaciers were exactly in-phase. This effect of
offsetting variability was especially strong in 2013, where early increases in D in the SE region dampened the winter
minimum. The seasonal amplitude of GrIS has also declined since 2013 due to the widespread, 20 % reduction in the
discharge seasonality of SE glaciers.

30 Changes in glacier discharge are due to changes in both ice flow speed and thickness, with less known about short-term
(seasonal to interannual) variations in the latter. Consistent with numerous studies (e.g. Helm et al. 2014; Csatho et al. 2014;
Kjeldsen et al. 2015), 89 % of the glaciers, including the 25 largest, thinned over the study period. Holding ice thickness



constant, so that the change in discharge is due entirely to changes in flow speed, results in an increase in D of 110 Gta⁻¹ by 2016, or 60 Gta⁻¹ greater than estimated when including ice thickness change (Figure S8). Thus, ice thinning has offset the increase in D due to ice flow acceleration by over 50 % since 2000, and this fraction is steadily increasing with time since the initial, rapid acceleration in the SE in 2002 and 2005. Ice thickness changes on sub-annual timescales also reduce the seasonal amplitude of D . Holding thickness constant, as above, results in a seasonal variation that is, on average, 10% larger than if thickness changes are included. Thus, inclusion of ice thickness change on sub-annual to decadal timescales is essential for accurate estimates of D .


Changes in ice thickness also modulate the relationship between changes in D and ice front position. As described in Sect. 3.3, cumulative annual front change and annual D are uncorrelated in the SE region. However, holding ice thickness constant, as above, results in a strong correlation ($r^2 = 0.79$, $p = 10^{-6}$), which is similar to that in the NW. Holding ice thickness constant (Figure S9b) also increases the strength of the correlation between annual changes in front position and the change in annual D the following year ($r^2 = 0.75$, $p = 10^{-5}$). These increased correlations reflect the expected dependence of ice velocity on changes in ice front position (e.g. Howat et al. 2008). The SE underwent a sudden, large increase in velocity and retreat in ice front position between 2002 and 2005, with another, smaller acceleration and retreat in 2010, but has remained largely stable since then. While velocity has remained stable, ice thinning has resulted in a declining D that is uncorrelated with cumulative ice front retreat. In contrast, both retreat and D have been increasing steadily in the NW throughout the record, indicating steadily increasing ice speeds, resulting in a high correlation between annual D and cumulative front position change (i.e. retreat).

Lastly, we expect glaciers to respond to changes in basal water pressure due to the seasonal input of runoff. While both D and meltwater runoff show a similar pattern of seasonal variability, with a possible relationship between the timing of the onset of runoff and the seasonal peak in D , neither the seasonal maximum in runoff, nor the seasonally-integrated runoff, are significantly correlated to annual D . These indicate a more complex interaction between runoff, ice flow velocity and D , where the rate and distribution of runoff into the subglacial system are more relevant to glacier flow than total runoff (Stearns and van der Veen, 2018). For example, the sensitivity of D to runoff may vary throughout the melt season, with increased sensitivity early in the melt season when drainage channels are inefficient and unable to support the influx of runoff into the system (Chandler et al. 2013), thus increasing water pressure at the bed and enhancing basal flow (Palmer et al. 2011; Bartholomew et al. 2010). This is consistent with 13 ± 9 day average lag in timing between the fastest increase in runoff and the maximum GrIS-wide D , which is close to the 18-day average “residence time” between the production of melt runoff on the ice sheet and its transport to the margin estimated by van Angelen et al. (2014). Thus, taking this residence time into account, the seasonal maximum flow speed, and therefore D , occurs near the time we would expect maximum pressurization of the subglacial drainage system. Future work will build on these concepts by closely examining discharge



rates of acceleration and deceleration in response to the distribution of runoff throughout the melt season, giving consideration to runoff residence times.

5 Conclusions



GrIS-wide D has remained near 490 Gta^{-1} following a period of rapid acceleration before 2006, representing an 11 % increase from . This apparent stabilization, however, is due to steady or declining flow speeds and ice thinning at the four largest glaciers, which dominate the ice sheet-wide total. Excluding these, the combined D of the remaining glaciers increased steadily over the time period, reaching a maximum in 2016, indicating that the largest glaciers are not representative of typical outlet glacier change. Trends in D vary regionally, increasing in the NW and NE and remaining steady in the SE, where sustained higher flow speeds are completely offset by ice thinning and D has returned to its year 2000 values. In total over the GrIS, ice thinning has offset the impact of increased ice flow speeds on D by over 50 % since 2000, substantially modulating the contribution of glacier dynamics on mass loss.

We find that annual changes in GrIS D can be mostly attributed to the cumulative, weighted change in glacier front position. This relationship is the strongest in the NW region, where continuous retreat has accompanied a near-linear increase in annual D and, therefore, changes in D are driven by changes in flow speed. In the SE, however, where speeds have remained relatively stable since 2005 while the glaciers have thinned, it is instead the annual changes in front position that correlate to changes in annual D the following year. In contrast, we find no correlations between annual D , or year-to-year changes in D , and modelled meltwater runoff. These results indicate that multi-year changes in D are dominated by changes in ice front position, through its impact to glacier dynamics, and that the magnitude of meltwater runoff has no consistent, discernible effect on total annual outlet glacier discharge.

We resolve a persistent, ubiquitous seasonal increase in D averaging 6 %. Regionally, this signal varies from 5 % in the SE to 9 % in the NW, with ± 1 -month differences in timing resulting in an offsetting effect that decreases the combined total. There was also a marked decline in seasonality after the period of rapid ice flow accelerations in the SE, resulting in a ~ 23 % decrease in seasonality after 2006, and a near complete disappearance of a seasonal signal in the SE after 2013. While not correlated on an annual basis, seasonal variations in D do correspond to those of runoff. We observe that maximum D occurs ~ 2 weeks after maximum increases in runoff, which is similar to the expected time for runoff to reach the margin, and ~ 2 weeks before the seasonal maximum runoff. We also observe significant correlation between the onset of runoff and the timing of peaks in D , with earlier-occurring runoff onset corresponding to earlier peaks in D . This is consistent with the expected impact of increasing meltwater input to an inefficient subglacial drainage system at the start of the melt season, increasing the subglacial water pressure and glacier sliding velocity. This is followed by a decline in D before the peak in runoff is reached, attributed to the transition to efficient subglacial drainage. Such a transition also may explain the lack of



correlation between the magnitudes of seasonal runoff and maximum D . Thus, while changes in front position, and their resulting persistent changes to the balance of forces at the glacier terminus, appear to dominant multi-year variability in regional and total GrIS D , seasonal variations are substantially controlled by the timing of meltwater input.

5 We have assessed the bulk behavior of ice sheet discharge and its broad relationships to possible external forcing, enabled by this first, complete estimate of continuous D over nearly two decades for all of Greenland's large marine terminating glaciers. It is well established, however, that the behavior of glaciers in close proximity and under similar environmental forcing can vary substantially (e.g. McFadden et al. 2011;  et al. 2012). This is likely due to the sensitivity of outlet glacier dynamics to their particularly geometry (e.g. Enderlin et al. 2013)  and we do not attempt to account for these differences here. However, detailed analysis of the relationships between particular glacier characteristics and their dynamics at a range of time scales using these data will be the subject of future work.

15

20

25

30



Author Contribution

MDK and IMH conceived this study and synthesized the required data sets. MDK performed the analyses and led writing the manuscript. SJ developed the orthorectified velocity maps and MJN developed algorithms for surface elevation, both used to derive the ice discharge estimations. BW processed and provided mass balance estimates derived from GRACE
5 observations, and BN and MRB developed the surface mass balance model, RACMO2.3p2, which was combined with discharge estimates to derive an ice sheet-wide record of mass balance. All authors contributed thoughtful discussions and insights to the study, and all authors contributed to editing the manuscript.

Acknowledgements

10 This work was supported by grants 80NSSC18K1027 and NNX13AI21A from the U.S. National Aeronautics and Space Administration and a fellowship from the Ohio State University.

Competing interests

The authors declare that they have no conflict of interest.

15

Data availability

All ice velocity and topographic products are publically available online. The velocity data maps and GIMP DEM are distributed through the NASA Distributed Active Archive Center at the NSIDC (<http://nsidc.org/data/measures/gimp>). Bed topography can also be accessed through the NSIDC portal at <https://nsidc.org/data/idbmg4>. Information on the
20 RACMO2.3p2 SMB data can be found at <http://www.projects.science.uu.nl/iceclimate/models/greenland.php>.

25



References

- Andersen, M. L., Nettles, M., Elosegui, P., Larsen, T. B., Hamilton, G. S. and Stearns, L. A.: Quantitative estimates of velocity sensitivity to surface melt variations at a large Greenland outlet glacier, *J. Glaciol.*, 57(204), 609–620, doi:10.3189/002214311797409785, 2011.
- 5
- Bartholomew, I., Nienow, P., Mair, D., Hubbard, A., King, M. A. and Sole, A.: Seasonal evolution of subglacial drainage and acceleration in a Greenland outlet glacier, *Nat. Geosci.*, 3, 408–411, doi:10.1038/ngeo863, 2010.
- Bendtsen, J., Mortensen, J., Lennert, K., Jens, K. E., Boone, W., Galindo, V., Hu, Y., Dmitrenko, I. A., Kirillov, S. A., Kjeldsen, K. K., Kristoff, Y., Barber, D. G. and Rysgaard, S.: Sea ice breakup and marine melt of a retreating tidewater outlet glacier in northeast Greenland (81 ° N), *Nature*, 1–11, doi:10.1038/s41598-017-05089-3, 2017.
- 10
- Bolch, T., Sandberg Sørensen, L., Simonsen, S. B., Mölg, N., MacHguth, H., Rastner, P. and Paul, F.: Mass loss of Greenland’s glaciers and ice caps 2003–2008 revealed from ICESat laser altimetry data, *Geophys. Res. Lett.*, 40(5), 875–881, doi:10.1002/grl.50270, 2013.
- 15
- Chandler, D. M., Wadham, J. L., Lis, G. P., Cowton, T., Sole, A., Bartholomew, I., Telling, J., Nienow, P., Bagshaw, E. B., Mair, D., Vinen, S. and Hubbard, A.: Evolution of the subglacial drainage system beneath the Greenland Ice Sheet revealed by tracers, *Nat. Geosci.*, 6, 195–198, doi:10.1038/ngeo1737, 2013.
- 20
- Choi, Y., Morlighem, M., Rignot, E., Mouginot, J., and Wood, M.: Modeling the Response of Nioghalvfjærdsfjorden and Zachariæ Isstrøm Glaciers, Greenland, to Ocean Forcing Over the Next Century, *Geophys. Res. Lett.*, 44, 11, 11–71, 79, doi:10.1002/2017GL075174, 2017.
- 25
- Csatho, B. M., Schenk, A. F., van der Veen, C. J., Babonis, G., Duncan, K., Rezvanbehbahani, S., van den Broeke, M. R., Simonsen, S. B., Nagarajan, S., and van Angelen, J. H.: Laser altimetry reveals complex pattern of Greenland ice sheet dynamics, *P. Natl. Acad. Sci. USA*, 111, 18478–18483, 2014.
- 30
- van As, D., Hasholt, B., Ahlstrøm, A. P., Box, J. E., Cappelen, J., Colgan, W., Fausto, R. S., Mernild, S. H., Mikkelsen, A. B., Noël, B. P. Y., Petersen, D. and van den Broeke, M. R.: Reconstructing Greenland Ice Sheet meltwater discharge through the Watson River (1949–2017), *Arctic, Antarct. Alp. Res.*, 50(1), S100010, doi:10.1080/15230430.2018.1433799, 2018.



- Enderlin, E. M., Howat, I. M., Jeong, S., Noh, M. J., Angelen, J. H. van, and van den Broeke, M. R.: An improved mass budget for the Greenland ice sheet, *Geophys. Res. Lett.*, 41, 1–7, doi.org/10.1002/2013GL059010, 2014.
- 5 Enderlin, E. M., Howat, I. M. and Vieli, A.: High sensitivity of tidewater outlet glacier dynamics to shape, *The Cryosphere*, [doi:10.5194/tc-7-1007-2013](https://doi.org/10.5194/tc-7-1007-2013), 2013.
- Fahnestock, M., Scambos, T., Moon, T., Gardner, A., Haran, T., and Klinger, M.: Rapid large-area mapping of ice flow using Landsat 8, *Remote Sens. Environ.*, 185, 84–94, doi.org/10.1016/j.rse.2015.11.023, 2016.
- 10 Hanna, E., Navarro, F. J., Pattyn, F., Domingues, C. M., Fettweis, X., Ivins, E. R., Nicholls, R. J., Ritz, C., Smith, B., Tulaczyk, S., Whitehouse, P. L., and Zwally, H. J.: Ice-sheet mass balance and climate change, *Nature*, 498, 51–59, 2013.
- Helm, V., Humbert, A., and Miller, H.: Elevation and elevation change of Greenland and Antarctica derived from CryoSat-2, *The Cryosphere*, 8, 1539–1559, [doi:10.5194/tc-8-1539-2014](https://doi.org/10.5194/tc-8-1539-2014), 2014.
- 15 Horgan, H. J., Anderson, B., Alley, R. B., Chamberlain, C. J., Dykes, R., Kehrl, L. M. and Townend, J.: Glacier velocity variability due to rain-induced sliding and cavity formation, *Earth Planet. Sci. Lett.*, [doi:10.1016/j.epsl.2015.10.016](https://doi.org/10.1016/j.epsl.2015.10.016), 2015.
- Howat, I. M., Joughin, I., Tulaczyk, S., and Gogineni, S.: Rapid retreat and acceleration of Helheim Glacier, east Greenland, *Geophys. Res. Lett.*, 32, L22502, [doi:10.1029/2005GL024737](https://doi.org/10.1029/2005GL024737), 2005.
- 20 Howat, I. M., Joughin, I. and Scambos, T. A.: Rapid changes in ice discharge from Greenland outlet glaciers, *Science*, 315, 1559–61, [doi:10.1126/science.1138478](https://doi.org/10.1126/science.1138478), 2007.
- 25 Howat, I. M., Joughin, I., Fahnestock, M., Smith, B. E., and Scambos, T. A.: Synchronous retreat and acceleration of southeast Greenland outlet glaciers 2000–06: ice dynamics and coupling to climate, *J. Glaciol.*, 54, 646–660, [doi:10.3189/002214308786570908](https://doi.org/10.3189/002214308786570908), 2008.
- Howat, I. M., Box, J. E., Ahn, Y., Herrington, A., and McFadden, E. M.: Seasonal variability in the dynamics of marine-terminating outlet glaciers in Greenland, *J. Glaciol.*, 56, 601–613, doi.org/10.3189/002214310793146232, 2010.
- 30 Howat, I. M., Ahn, Y., Joughin, I., van den Broeke, M. R., Lenaerts, J. T. M., and Smith, B.: Mass balance of Greenland’s three largest outlet glaciers, 2000–2010, *Geophys. Res. Lett.*, 38, L12501, [doi:10.1029/2011GL047565](https://doi.org/10.1029/2011GL047565), 2011.



- Howat, I. M., Negrete, A., and Smith, B. E.: The Greenland Ice Mapping Project (GIMP) land classification and surface elevation data sets, *The Cryosphere*, 8, 1509–1518, doi.org/10.5194/tc-8-1509-2014, 2014.
- Jeong, S., Howat, I. M. and Ahn, Y.: Improved Multiple Matching Method for Observed Glacier Motion with Repeat Image
5 Feature Tracking, *IEEE Trans. Geosci. Remote Sens.*, 55, 2431–2441, 2017.
- Jeong, S. and Howat, I. M.: Performance of Landsat 8 Operational Land Imager for mapping ice sheet velocity, *Remote Sens. Environ.*, 170, 90–101, [doi:10.1016/j.rse.2015.08.023](https://doi.org/10.1016/j.rse.2015.08.023), 2015.
- 10 Jones, S. D., Le Quéré, C., Rödenbeck, C., Manning, A. C. and Olsen, A.: A statistical gap-filling method to interpolate global monthly surface ocean carbon dioxide data, *J. Adv. Model. Earth Syst.*, 7, 1554–1575, [doi:10.1002/2014MS000416](https://doi.org/10.1002/2014MS000416), 2015.
- Joughin, I., Abdalati, W., and Fahnestock, M.: Large fluctuations in speed on Greenland’s Jakobshavn Isbræ glacier, *Nature*,
15 432, 608–610, [doi:10.1038/nature03130](https://doi.org/10.1038/nature03130), 2004.
- Joughin, I., Das, S. B., King, M. A., Smith, B. E., Howat, I. M., and Moon, T.: Seasonal Speedup Along the Western Flank of the Greenland Ice Sheet, *Science*, 320, 781–784, doi.org/10.1126/science.1153288, 2008.
- 20 Joughin, I., Smith, B. E., Howat, I. M., Floricioiu, D., Alley, R. B., Truffer, M., and Fahnestock, M.: Seasonal to decadal scale variations in the surface velocity of Jakobshavn Isbræ, Greenland: Observation and model-based analysis, *J. Geophys. Res.-Earth Surf.*, 117, 1–20, doi.org/10.1029/2011JF002110, 2012.
- Joughin, I., B. Smith, B., Howat, I., and Scambos, T.: MEaSURES Greenland Ice Sheet Velocity Map from InSAR Data,
25 Version 2. Boulder, Colorado USA. NASA National Snow and Ice Data Center Distributed Active Archive Center, 2015, updated 2017.
- Khan, S. A., Sasgen, I., Bevis, M., van Dam, T., Bamber, J. L., Wahr, J., Willis, M., Kjaer, K. H., Wouters, B., Helm, V., Csatho, B., Fleming, K., Bjork, A. A., Aschwanden, A., Knudsen, P. and Munneke, P. K.: Geodetic measurements reveal
30 similarities between post-Last Glacial Maximum and present-day mass loss from the Greenland ice sheet, *Sci. Adv.*, 2(9), e1600931–e1600931, [doi:10.1126/sciadv.1600931](https://doi.org/10.1126/sciadv.1600931), 2016.
- Kjeldsen, K. K., Korsgaard, N. J., Bjørk, A. A., Khan, S. A., Box, J. E., Funder, S., Larsen, N. K., Bamber, J. L., Colgan, W., van den Broeke, M. R., Siggaard-Andersen, M.L., Nuth, C., Schomacker, A., Andresen, C. S., Willerslev, E., and Kjær, K.



- H.: Spatial and temporal distribution of mass loss from the Greenland ice sheet since AD 1900, *Nature*, 528, 396–400, doi:10.1038/nature16183, 2015.
- Korona, J., Berthier, E., Bernard, M., Rémy, F. and Thouvenot, E.: SPIRIT. SPOT 5 stereoscopic survey of Polar Ice: Reference Images and Topographies during the fourth International Polar Year (2007–2009), *ISPRS J. Photogramm. Remote Sens.*, 64, 204–212, doi.org/10.1016/j.isprsjprs.2008.10.005, 2009.
- Krimmel, R., and Rasmussen, L.: Using sequential photography to estimate ice velocity at the terminus of Columbia Glacier, Alaska. *Ann. Glaciol.*, 117–123, 1985.
- 10 Lemos, A., Shepherd, A., McMillan, M., Hogg, A. E., Hatton, E. and Joughin, I.: Ice velocity of Jakobshavn Isbræ, Petermann Glacier, Nioghalvfjærdsfjorden and Zachariæ Isstrøm, 2015–2017, from Sentinel 1-a/b SAR imagery, *Cryosph. Discuss.*, 2087–2097 [online], doi.org/10.5194/tc-2017-251, 2018.
- 15 McFadden, E. M., Howat, I. M., Joughin, I., Smith, B. E. and Ahn, Y.: Changes in the dynamics of marine terminating outlet glaciers in west Greenland (2000–2009), *J. Geophys. Res. Earth Surf.*, 116, 1–16, doi:10.1029/2010JF001757, 2011.
- Moon, T. and Joughin, I.: Changes in ice front position on Greenland’s outlet glaciers from 1992 to 2007, *J. Geophys. Res. Earth Surf.*, 113, F2, doi:10.1029/2007JF000927, 2008.
- 20 Moon, T., Joughin, I., Smith, B., and Howat, I.: 21st-century evolution of Greenland outlet glacier velocities, *Science*, 336, 576– 578, doi.org/10.1126/science.1219985, 2012.
- Moon, T., Joughin, I., Smith, B., van den Broeke, M. R., Berg, W. J., Noël, B., and Usher, M.: Distinct patterns of seasonal Green- land glacier velocity, *Geophys. Res. Lett.*, 41, 7209–7216, doi.org/10.1002/2014GL061836, 2014.
- 25 Moon, T., Joughin, I., and Smith, B.: Seasonal to multiyear variability of glacier surface velocity, terminus position, and sea ice/ice mélange in northern Greenland, *J. Geophys. Res. Earth Surf.*, 120, 818–833, doi.org/10.1002/2015JF003494, 2015.
- 30 Morlighem, M., Williams, C. N., Rignot, E., An, L., Arndt, J. E., Bamber, J. L., Catania, G., Chauché, N., Dowdeswell, J. A., Dorschel, B., Fenty, I., Hogan, K., Howat, I., Hubbard, A., Jakobsson, M., Jordan, T. M., Kjeldsen, K. K., Millan, R., Mayer, L., Mouginot, J., Noël, B. P. Y., O’Cofaigh, C., Palmer, S., Rysgaard, S., Seroussi, H., Siegert, M. J., Slabon, P., Straneo, F., van den Broeke, M. R., Weinrebe, W., Wood, M. and Zinglensen, K. B.: BedMachine v3: Complete Bed



- Topography and Ocean Bathymetry Mapping of Greenland From Multibeam Echo Sounding Combined With Mass Conservation, *Geophys. Res. Lett.*, 44, 11,051-11,061, doi:10.1002/2017GL074954, 2017.
- 5 Mougnot, J., Rignot, E., Scheuchl, B., Fenty, I., Khazendar, A., Morlighem, M., and Paden, J.: Fast retreat of Zachariæ Isstrøm, northeast Greenland, *Science*, 250, 1357-1361, doi.org/10.1126/science.aac7111, 2015.
- Motyka, R. J., Cassotto, R., Truffer, M., Kjeldsen, K. K., Van As, D., Korsgaard, N. J., Fahnestock, M., Howat, I., Langen, P. L., Mortensen, J., Lennert, K. and Rysgaard, S.: Asynchronous behavior of outlet glaciers feeding Godthåbsfjord (Nuup Kangerlua) and the triggering of Narsap Sermia's retreat in SW Greenland, *J. Glaciol.*, 63(238), 288–308,
10 doi:10.1017/jog.2016.138, 2017.
- Münchow, A., Padman, L., and Fricker, H. A.: Interannual changes of the floating ice shelf of Petermann Gletscher, North Greenland, from 2000 to 2012, *J. Glaciol.*, 60, 489–499, doi.org/10.3189/2014JoG13J135, 2014.
- 15 Noh, M. J. and Howat, I.: Automated Coregistration of Repeat Digital Elevation Models for Surface Elevation Change Measurement Using Geometric Constraints, *IEEE Trans. Geosci. Remote Sens.*, 52, 2247–2260, doi:10.1109/TGRS.2013.2258928, 2014.
- Noh, M.J. and Howat, I.: Automated stereo-photogrammetric DEM generation at high latitudes: Surface Extraction with
20 TIN-based Search-space Minimization (SETSM) validation and demonstration over glaciated regions, *GIScience & Remote Sens.*, 52:2, 198-217, doi:10.1080/15481603.2015.1008621, 2015.
- Nguyen, A. T. and Herring, T. A.: Analysis of ICESat data using Kalman filter and kriging to study height changes in East Antarctica, *Geophys. Res. Lett.*, 32, 4–7, doi:10.1029/2005GL024272, 2005.
25
- Noël, B., van de Berg, W. J., Machguth, H., Lhermitte, S., Howat, I., Fettweis, X., and van den Broeke, M. R.: A daily, 1 km resolution data set of downscaled Greenland ice sheet surface mass balance (1958–2015), *The Cryosphere*, 10, 2361-2377, doi.org/10.5194/tc-10-2361-2016, 2016.
- 30 Noël, B., van de Berg, W. J., van Wessem, J. M., van Meijgaard, E., van As, D., Lenaerts, J. T. M., Lhermitte, S., Kuipers Munneke, P., Smeets, C. J. P. P., van Ulf, L. H., van de Wal, R. S. W., and van den Broeke, M. R.: Modelling the climate and surface mass balance of polar ice sheets using RACMO2 – Part 1: Greenland (1958–2016), *The Cryosphere*, 12, 811-831, doi.org/10.5194/tc-12-811-2018, 2018.



- Palmer, S., Shepherd, A., Nienow, P. and Joughin, I.: Seasonal speedup of the Greenland Ice Sheet linked to routing of surface water, *Earth Planet. Sci. Lett.*, 302, 423–428, doi:10.1016/j.epsl.2010.12.037, 2011.
- Pritchard, H. D., Arthern, R. J., Vaughan, D. G. and Edwards, L. A.: Extensive dynamic thinning on the margins of the Greenland and Antarctic ice sheets, *Nature*, 461, 971–975, doi.org/10.1038/nature08471, 2009.
- 5 Rignot, E. and Kanagaratnam, P.: Changes in the Velocity Structure of the Greenland Ice Sheet, *Science*, 311, 986–990, doi.org/10.1126/science.1121381, 2006.
- Rignot, E., Box, J. E., Burgess, E., and Hanna, E.: Mass balance of the Greenland ice sheet from 1958 to 2007, *Geophys. Res. Lett.*, 35, L20502, doi:10.1029/2008GL035417, 2008.
- 10 Rignot, E., Velicogna, I., van den Broeke, M. R., Monaghan, A., and Lenaerts, J. T. M.: Acceleration of the contribution of the Greenland and Antarctic ice sheets to sea level rise, *Geophys. Res. Lett.*, 38, L05503, doi:10.1029/2011GL046583, 2011.
- 15 Rosenau, R., Scheinert, M. and Dietrich, R.: A processing system to monitor Greenland outlet glacier velocity variations at decadal and seasonal time scales utilizing the Landsat imagery, *Remote Sens. Environ.*, 169, 1–19, doi:10.1016/j.rse.2015.07.012, 2015.
- Sasgen, I., van den Broeke, M. R., Bamber, J. L., Rignot, E., Sørensen, L. S., Wouters, B., Martinec, Z., Velicogna, I., and Simonsen, S. B.: Timing and origin of recent regional ice-mass loss in Greenland, *Earth Planet. Sc. Lett.*, 333–334, 293–303, 2012.
- 20 Stearns, L. A. and van der Veen, C. J.: Friction at the bed does not control fast glacier flow, *Science*, doi:10.1126/science.aat2217, 2018.
- 25 Straneo, F. and Heimbach, P.: North Atlantic warming and the retreat of Greenland’s outlet glaciers., *Nature*, 504, 36–43, doi:10.1038/nature12854, 2013.
- Thomas, R. H.: Force-perturbation analysis of recent thinning and acceleration of Jakobshavn Isbræ, Greenland, *J. Glaciol.*, 50, 57– 66, 2004.
- 30 van Angelen, J. H., van den Broeke, M. R., Wouters, B. and Lenaerts, J. T. M.: Contemporary (1960–2012) Evolution of the Climate and Surface Mass Balance of the Greenland Ice Sheet, *Surv. Geophys.*, 35(5), 1155–1174, doi:10.1007/s10712-013-9261-z, 2014.



van den Broeke, M. R., Enderlin, E., Howat, I., Kuipers Munneke, P., Noël, B., van de Berg, W. J., van Meijgaard, E. and Wouters, B.: On the recent contribution of the Greenland ice sheet to sea level change, *The Cryosphere*, 10, 1933–1946, doi:10.5194/tc-10-1933-2016, 2016.

5

Walsh, K. M., Howat, I. M., Ahn, Y. and Enderlin, E. M.: Changes in the marine-terminating glaciers of central east Greenland, 2000–2010, *The Cryosphere*, doi:10.5194/tc-6-211-2012, 2012.

10 Vaughan, D. G., Comiso, J. C., Allison, I., Carrasco, J., Kaser, G., Kwok, R., Mote, P., Murray, T., Paul, F., Ren, J., Rignot, E., Solomina, O., Steffen, K., and Zhang, T.: Observations: Cryosphere, in: *Climate Change 2013: The Physical Science Basis. Contribution of Working Group I to the Fifth Assessment Report of the Intergovernmental Panel on Climate Change*, edited by: Stocker, T. F., Qin, D., Plattner, G. K., Tignor, M., Allen, S. K., Boschung, J., Nauels, A., Xia, Y., Bex, V., and Midgley, P. M., 4, 317–382, Cambridge University Press, 2013.

15 Wouters, B., Bamber, J. L., van den Broeke, M. R., Lenaerts, J. T. M., and Sasgen, I.: Limits in detecting acceleration of ice sheet mass loss due to climate variability, *Nat. Geosci.*, 6, 613–616, 2013.

20

25

30

35



5 **Table 1: GrIS-wide and basin-scale (delineated in Fig. S6) cumulative mass changes in Gigatons over the 2003–2016 period, listed as the RACMO2.3p2 SMB component, SMB– D mass balance, and GRACE mass balance estimates. Cumulative mass changes here represent the difference between mean annual 2016 and mean annual 2003 estimates, with a negative value indicating net mass loss. The GrIS* domain includes SMB fields from tundra and detached ice caps.**

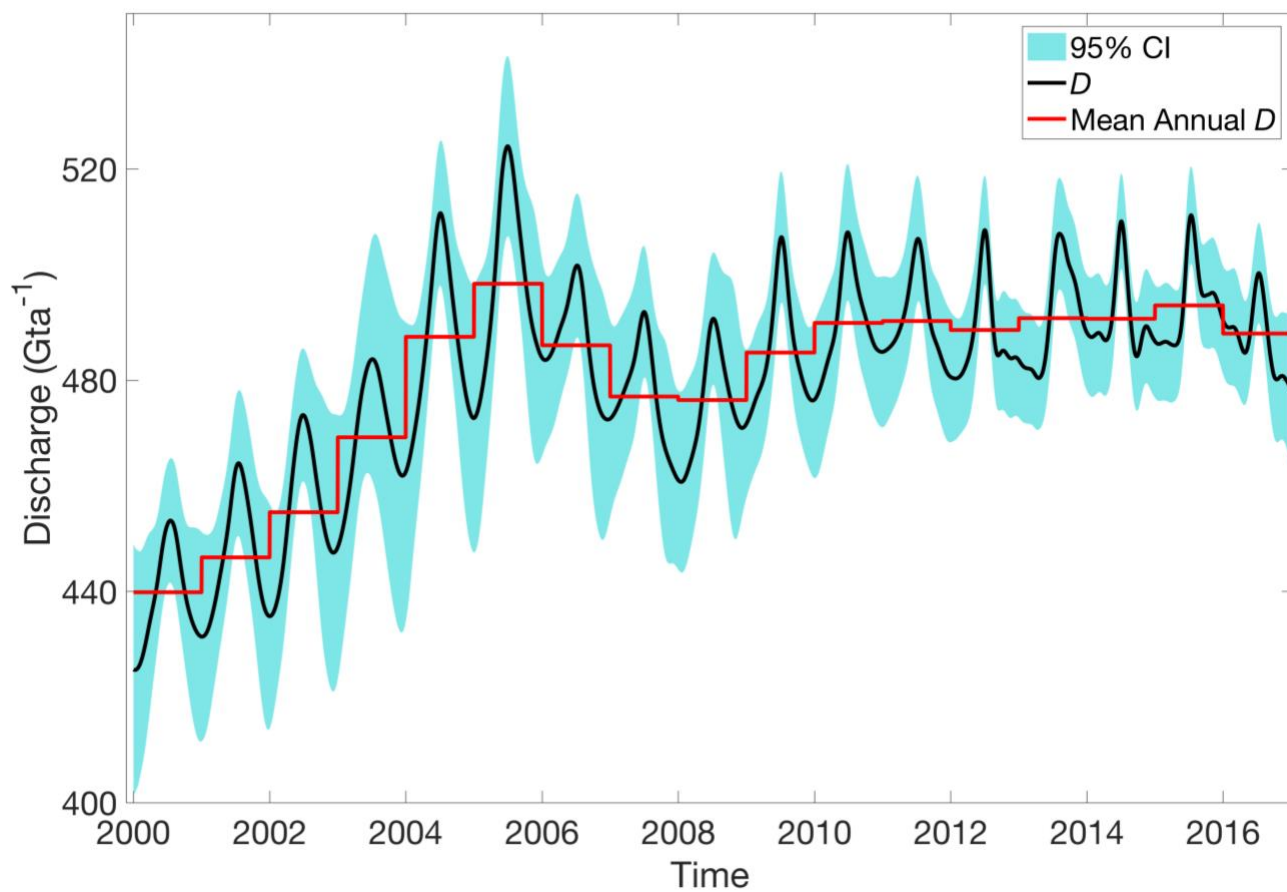
	SMB	SMB– D	GRACE
Basin 1	-45 ± 31	-334 ± 32	-202 ± 5
Basin 2	155 ± 42	-266 ± 43	-159 ± 10
Basin 3	744 ± 42	-400 ± 43	-447 ± 38
Basin 4	1645 ± 46	-476 ± 48	-922 ± 34
Basin 5	502 ± 69	-869 ± 71	-841 ± 80
Basin 6	558 ± 27	-823 ± 28	-910 ± 44
GrIS*	3458 ± 258	-3263 ± 259	-3479 ± 280

10 **Table 2: Summary of D values for the total GrIS and four distinct regions (see Fig. 3), including the estimated mean annual D in 2000, the maximum D over the 2000–2016 period, and the cumulative D anomaly (ΔD_{2000}) relative to the 2000 estimate. All values are described in units of Gta^{-1} . A negative value indicates a reduction in D relative to the 2000 value.**

	2000 D	MAXIMUM D	ΔD_{2000}
southwest	9.5 ± 1	10 ± 1	-7 ± 3
southeast	182 ± 6	238 ± 4	284 ± 17
northeast	53 ± 2	63 ± 2	47 ± 8
northwest	187 ± 5	240 ± 3	343 ± 21
GrIS	440 ± 8	524 ± 9	682 ± 31

15

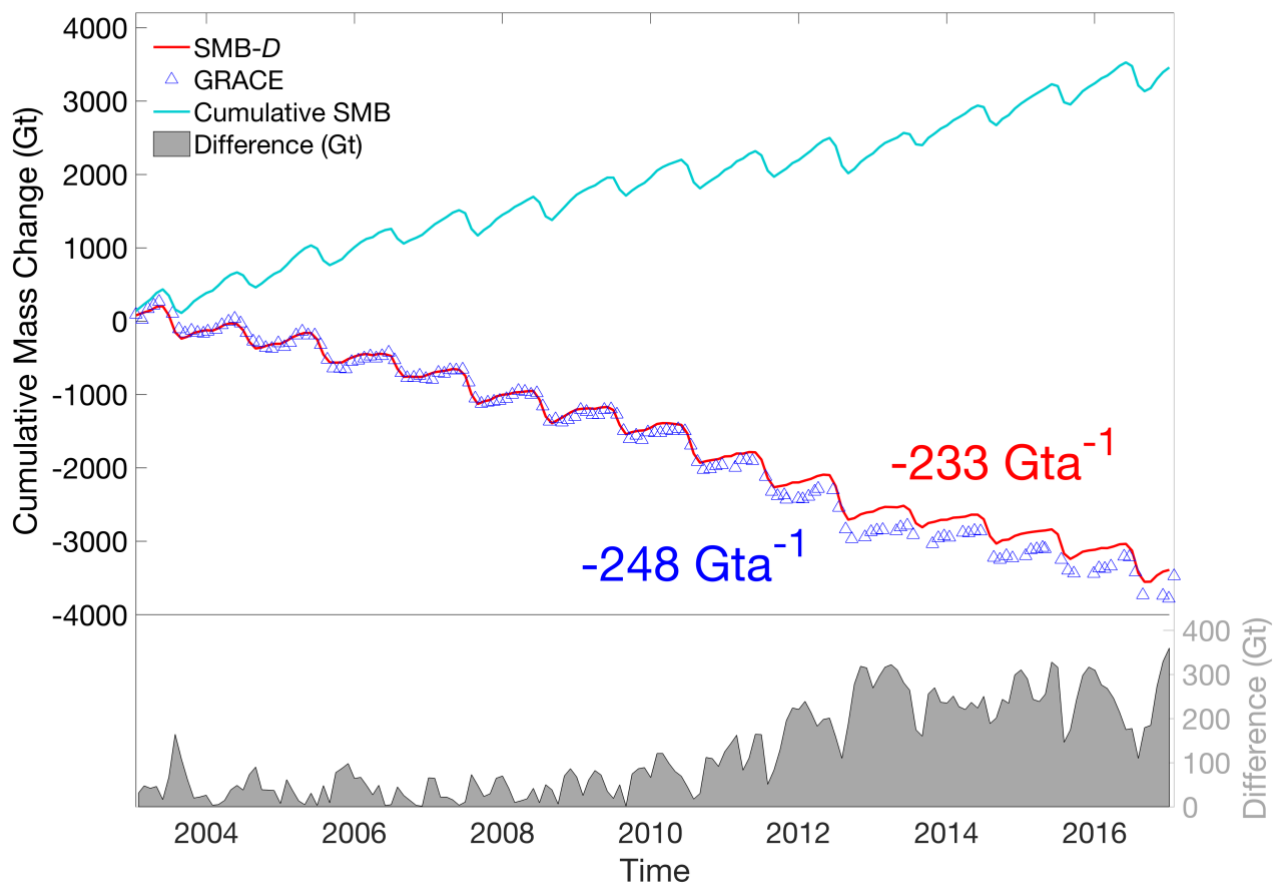
20



5 **Figure 1: Continuous estimates of discharge, D , for the GrIS for the 2000–2016 period, expressed as a rate of Gigatons per year (Gta^{-1}). Shading represents the 95% confidence interval.**

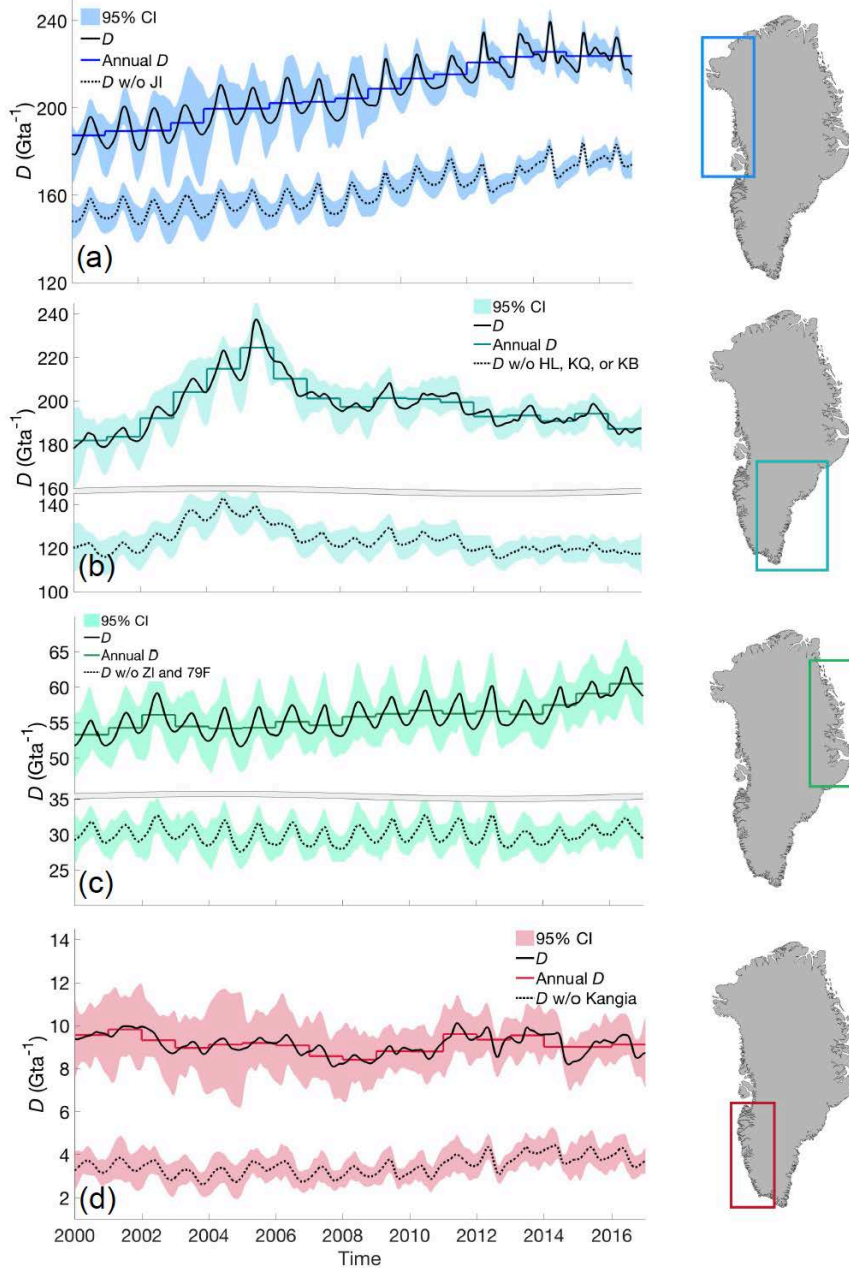
10

15

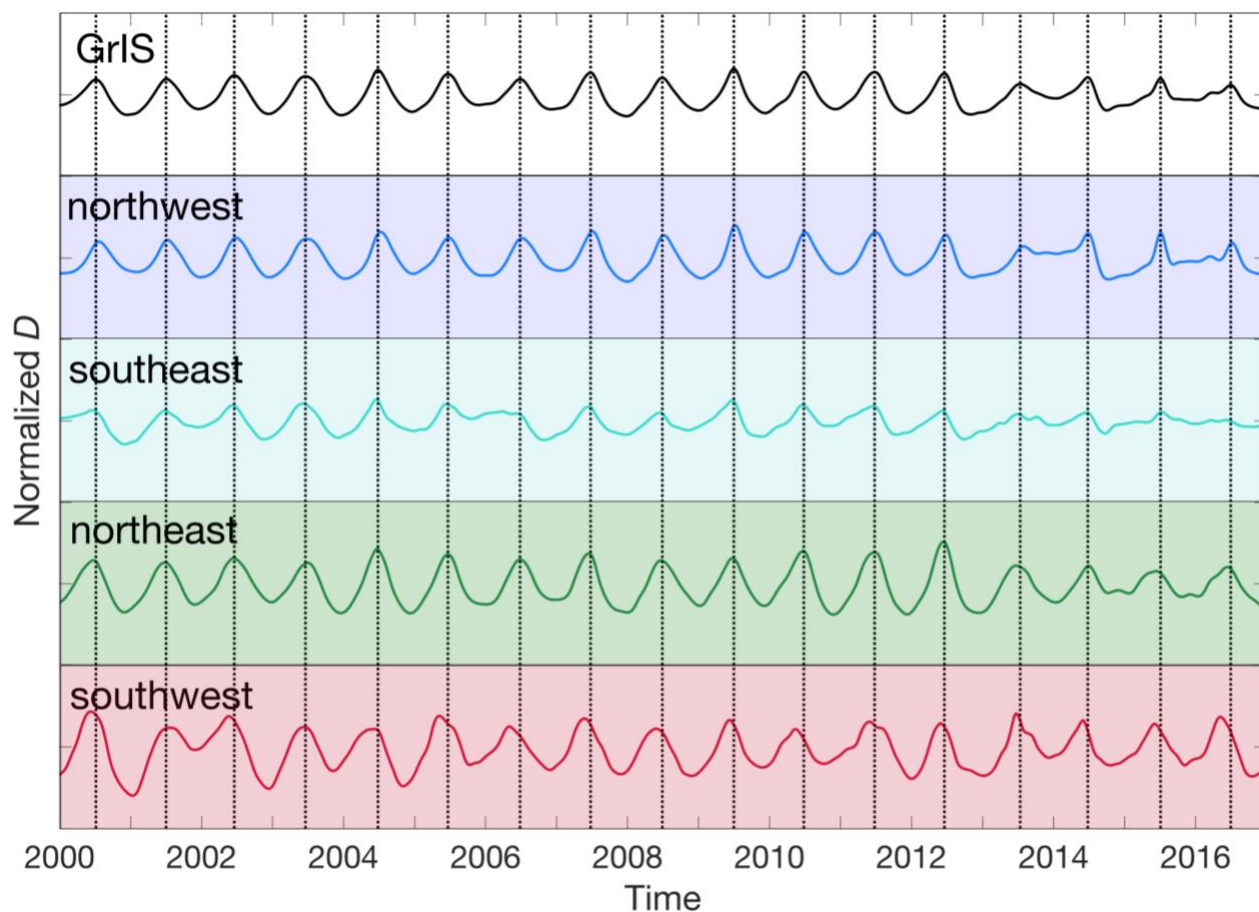


5

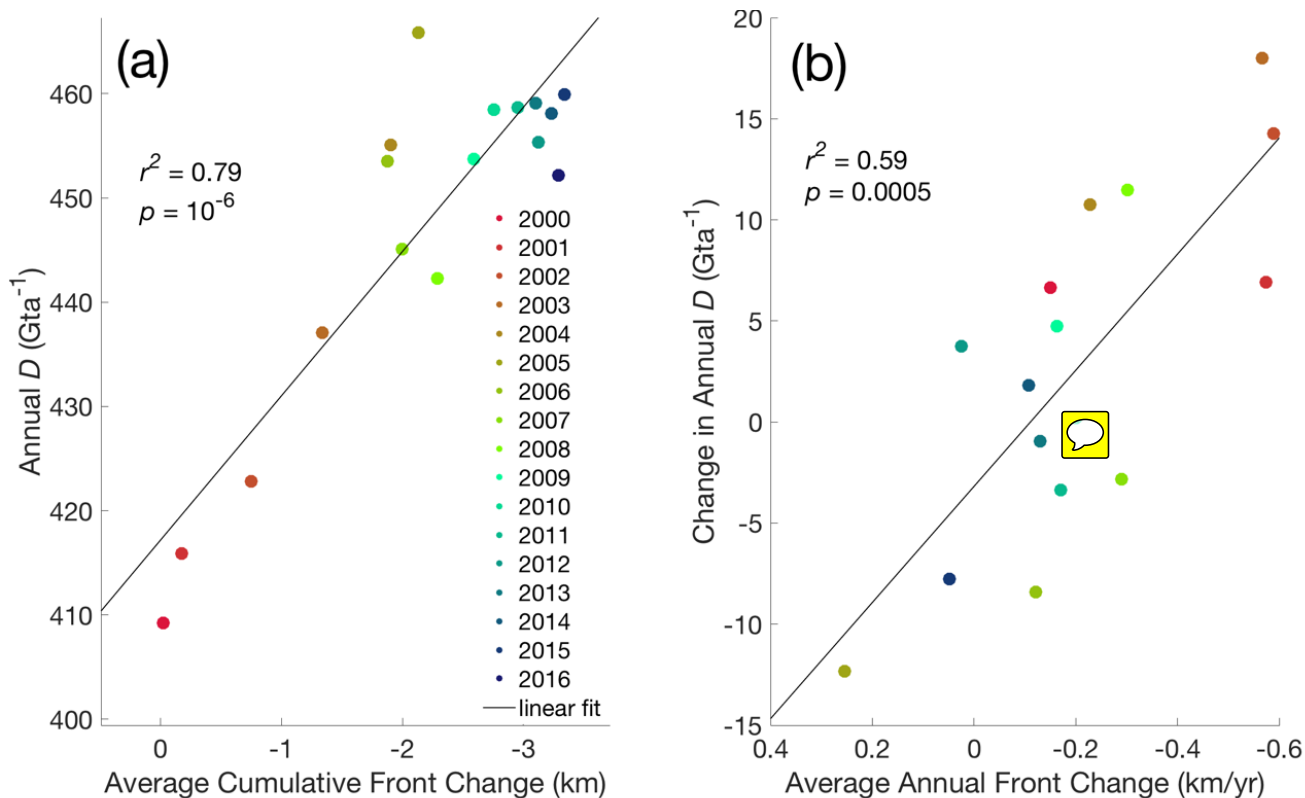
Figure 2: Comparative cumulative GrIS mass change relative to 2003 between GRACE and monthly SMB-D. Cumulative SMB is also plotted, with cumulative differences between estimates plotted in the lower panel, associated with the right y-axis.



5 **Figure 3: Net regional D including (solid line) and excluding (dashed line) the dominant glaciers in each region, with shading representing the 95% confidence interval. From top to bottom these regions include: The northwest (a), plotted with and without Jakobshavn (JI), the southeast (b) with and without Helheim (HL), Kangerdlugssuaq (KQ), and the main trunk of Køge Bugt (KB), the northeast (c), with and without Zachariae Isstrøm (ZI) and 79Fjorden (79F), and the southwest (d) with and without Kangia Glacier.**



5 **Figure 4: Normalized, detrended D time series for the total GrIS (top), NW (blue), SE (cyan), NE (green) and SW (red) regions. The normalized discharge within each panel spans from -1 to 1 . Vertical black lines align with the annual maximum D of the GrIS-wide series.**



5 **Figure 5:** (a) Colored dots are GrIS cumulative average front position change since 1 January 2000, with negative indicating retreat, versus annual average discharge, D , for each year between 2000 and 2016. The black line is the linear best fit to the data points, with the variance (r^2) and probability value (p) of the fit labelled. (b) The average rate of front position change, with negative values indicating retreat, for each year versus the change in average annual discharge between years. Point color scale, line, and statistics are the same as for (a).

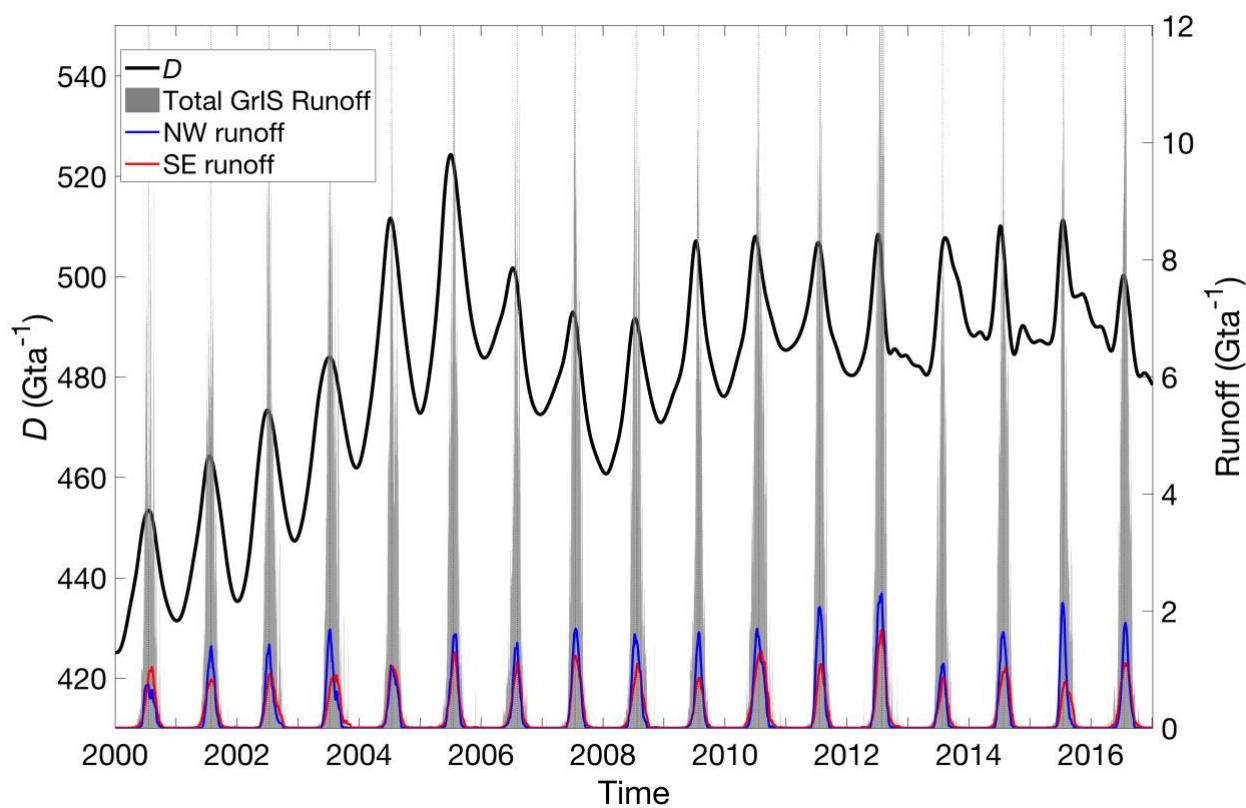


Figure 6: Cumulative GrIS D (black, left y-axis) plotted with raw daily runoff totals (gray bars, right y-axis). The timing of the seasonal maximum runoff is emphasized by vertical dotted lines. Regional runoff totals, smoothed by a 31-day running mean, are shown for the NW and SE region.

5

10